Role of tin clustering in band structure and thermodynamic stability of GeSn by atomistic modeling

Running title: Effect of tin clustering in GeSn materials

Running Authors: Karthikeyan and Hudait

Sengunthar Karthikeyan <sup>1</sup> and Mantu K. Hudait <sup>1,a)</sup>

<sup>1</sup>Advanced Devices & Sustainable Energy Laboratory (ADSEL), Bradley Department of Electrical and Computer Engineering, Virginia Polytechnic Institute and State University, Blacksburg,

Virginia (VA) 24061, USA.

a) Electronic mail: mantu.hudait@vt.edu

hindered by various factors such as Sn segregation, clustering, and short-range ordering

**ABSTRACT:** Synthesis of device-quality GeSn materials with higher Sn compositions is

effects. In the present work, the impact of the clustering of Sn atoms in a GeSn

semiconductor alloy was studied by density functional theory (DFT) using SG15

pseudopotentials in Synopsys QuantumATK tool. Where, the thermodynamic stability,

effective band structure, indirect and direct band gaps, and density of states (DOS), were

computed to highlight the difference between a cluster-free random GeSn alloy and a GeSn

alloy with Sn–Sn clusters. A 54-atom bulk  $Ge_{1-x}Sn_x$  (x = 3.71 % to 27.77 %) supercell was

constructed with cluster-free and a 1<sup>st</sup> nearest neighbor (NN) Sn-Sn clustered GeSn alloy

at each composition for this work. Computation using the generalized gradient

approximation exchange-correlation functional showed thermodynamic stability of GeSn

was reduced due to the clustering of Sn, that increased the formation energy of the GeSn

alloys, by increasing the Hartree potential energy and exchange-correlation energy.

Moreover, the effective band structure of GeSn material at a Sn composition of ~22%, both

direct  $(E_{g, \Gamma})$  and indirect  $(E_{g, L})$  band gaps decreased by a large margin of 40.76 meV and

1

120.17 meV, respectively due to Sn–Sn clustering. On the other hand, the  $E_g$ ,  $\Gamma$  and  $E_g$ , Ldecrease is limited to 0.5 meV and 12.8 meV, respectively, for Sn composition of ~5.6%. Similar impacts were observed on DOS, in an independent computation without deducing from the electronic band structure, where the width of the forbidden band reduces due to the clustering of Sn atoms in GeSn. Moreover, using the energy band gaps of GeSn computed with the assumption of it being a random alloy having well dispersed Sn atoms needs revision by incorporating clustering, to align with the experimentally determined band gaps. This necessitates incorporating the effect of Sn atoms clustered together at varying distributions based on experimental characterization techniques such as atom probe tomography or extended x-ray absorption fine structure to substantiate the energy band gap of GeSn alloy at a particular composition with precision. Hence, considering the effect of Sn clusters during material characterization, beginning with the accurate energy band gap characterization of GeSn would help in mitigating the effect of process variations on the performance characteristics of GeSn-based group IV electronic and photonic devices such as varying leakage currents in transistors and photodiodes as well as the deviation from the targeted wavelength of operation in lasers and photodetectors.

#### I. INTRODUCTION

To realize highly efficient group IV semiconductor-based optoelectronic devices, significant advancements in the quality of SiGe, SiGeSn, GeSn, and strained Ge<sup>1-15</sup> materials are essential. Alloying α-Sn with Ge can make GeSn a direct band gap semiconductor at 6% to 8% Sn composition, 1-11 where different Sn alloy compositions were reported for the indirect to direct band gap transition based on the first-principles calculations.<sup>2, 16, 17</sup> In addition, recent studies predicted a near-zero band gap GeSn material at Sn composition in the range of 25–28%. 2, 16, 17 Further, there are also reports of GeSn material continuing to behave as a semiconductor even at 32% Sn<sup>18</sup> based on the ordering of atoms. These developments have added challenges in characterizing GeSn materials at high Sn compositions due to the segregation of Sn (i.e., Sn atoms clustering), creation of point defects, lattice mismatch induced defects and dislocations, etc. 19-22 However, there are very few studies reporting the effect of Sn clustering in GeSn materials.<sup>23–25</sup> The GeSn alloy has been considered a truly random alloy like SiGe<sup>25</sup> while computing the energy band gaps from the first-principles calculations and the corresponding compositions are calibrated with experimentally determined energy band gaps. There is a need to initiate a revision of electronic band structure computation by incorporating the clustering of Sn atoms. For instance, the localized Sn composition in a cluster within GeSn alloy is reported to be even greater than the average Sn composition using atom probe tomography (APT). <sup>26, 27</sup> Also reported is increased clustering at compositions greater than 12% using extended X-ray absorption fine structure (EXAFS).<sup>28</sup> In the present work, the clustering of Sn atoms in GeSn alloy is studied by density functional theory (DFT) using the Synopsys QuantumATK tool: (i) to compute the effective band structure (both indirect and direct

energy band gaps), understand the thermodynamic stability of the many-electron system with respect to the formation energy and compute density of states (DOS) for clustered GeSn; (ii) within an integrated tool that facilitates studying atomic-scale effects at materials, devices, and circuit levels on the same platform.<sup>29</sup> The result exhibited a lowering in the indirect-direct energy band gaps and reduced thermodynamical stability with higher formation energy due to the clustering of Sn atoms in a GeSn alloy. Note that only 1st nearest neighbor (1st-NN) Sn-Sn clusters were modeled in the present work, with the maximum cluster size equaling the localized and average Sn composition in a 54-atom GeSn supercell. For clarity, the distribution of Sn atoms in a cluster as  $m^{th}$ -NN (m > 1) was not modeled here. Results from APT have reported ~14%, ~21%, and even ~39% localized Sn composition in a  $\sim$ 7% average Sn compositional GeSn alloy with peak fraction of Sn atoms as 1<sup>st</sup>-NN.<sup>26</sup> Moreover, the Sn-Sn clusters have a Poisson distribution<sup>27</sup> (bellshaped), and the same has been used in the present work. Hence, this work would help to initiate necessary revisions in the electronic band structure computation of GeSn alloy by incorporating Sn clusters and open up further investigations with intricate cluster characterization techniques to minimize clustering at higher Sn compositions in GeSn semiconductor materials systems.

#### II. MODELLING METHODOLOGY

# A. Density-Functional Method

Density functional theory based on the Kohn-Sham  $(KS)^{30-34}$  mathematical formalism was implemented in the present work to study the clustering of Sn atoms with  $1^{st}$ -NN Sn-Sn clusters in the  $Ge_{1-x}Sn_x$  material system. The generalized gradient approximation (GGA) exchange-correlation functional of PBE<sup>35</sup> was applied using

Synopsys QuantumATK<sup>36</sup> tool to compute the electronic band structure and the density of states. The KS Hamiltonian is expressed as:<sup>35</sup>

$$\hat{\mathbf{H}}^{KS} = -\frac{\hbar^2}{2m} \nabla^2 + V_{eff},\tag{1}$$

where,  $V_{eff}$  is the effective potential of the electronic system and is expressed as:<sup>35</sup>

$$V_{eff}[n] = V_{H}[n] + V_{XC}[n] + V_{ext}[n]$$
 (2)

where, n is the electron density,  $V_H$  is Hartree potential representing electrostatic interaction between the electrons,  $V_{XC}$  is exchange-correlation potential representing the quantum mechanical nature of the electrons, and  $V_{ext}$  represents the electrostatic potential of the ions as well as any externally applied electrostatic fields. The total energy of the many-electron system ( $E_{Total}$ ) includes contributions from all these potentials, referred to above, and kinetic energy.

Furthermore, the thermodynamic stability of GeSn alloy was studied using the formation energy of the material, lower formation energy indicates better thermodynamic stability.<sup>37–39</sup> In the electronic structure calculations, the formation energy has been directly evaluated from the total energy<sup>38–41</sup> using the relation:

$$E_{Form} = E_{Total} - \sum_{x} E_{Total}(x), \tag{3}$$

where,  $E_{Form}$  is the formation energy of the alloy,  $E_{Total}$  is the total energy of the alloy and last term denotes the energy of the source elements. Here, the  $E_{Form}$  of GeSn alloy is given as:

$$E_{Form}^{GeSn} = E_{Total}^{GeSn} - \{ E_{Total}(Ge) + E_{Total}(Sn) \}, \tag{4}$$

where, the terms  $E_{Total}(Ge)$  and  $E_{Total}(Sn)$  represent the energy associated with the flux coming from the individual Ge and Sn effusion cells. Moreover, the number of Ge and Sn atoms was kept the same in both the cluster-free and 1<sup>st</sup>-NN Sn-Sn clustered GeSn alloys.

Hence, the change in the total energy  $\Delta E_{Total}$  is equivalent to the change in the formation energy  $\Delta E_{Form}$ . These changes result from the variation in the types of bonds (Ge–Ge, Ge–Sn, and Sn–Sn) between a truly random and clustered GeSn alloy. The total energy,  $E_{Total}$ , of a many electron-system is expressed in terms of the electron density (n) function as:<sup>35</sup>

$$E_{Total}[n] = T[n] + E_{H}[n] + E_{XC}[n] + E_{ext}[n],$$
 (5)

where, T[n] is the kinetic energy,  $E_H[n]$  is the Hartree potential energy,  $E_{XC}[n]$  is the exchange-correlation energy and  $E_{ext}[n]$  is the interaction energy due to external potential,  $V_{ext}$ . Here, the solution for  $V_H$  from the Poisson equation:<sup>36</sup>

$$\nabla^2 V_H[n](r) = -\frac{e^2}{4\pi\varepsilon_0} n(r), \tag{6}$$

shows that  $E_H$  is a functional of the local electron density only and not its gradient as in the GGA functional that is a semi-local approximation for  $E_{XC}$ , where it depends on both the local value (n) and the local gradient of the electron density  $(\nabla n)$  as shown below:<sup>36</sup>

$$E_{XC}[n] = \int n(r) \varepsilon^{XC} (n(r), \nabla n(r)) dr.$$
 (7)

During the DFT computation, the ground state of the electronic system is computed by iteratively minimizing  $E_{Total}$  of the system, at which the system is at its energetically and thermodynamically stable condition.<sup>36</sup>

In the present work, a norm-conserving scalar-relativistic (SG15) pseudopotential was used along with the linear combination of atomic orbitals (LCAO) basis sets as eigenfunctions of the KS Hamiltonian. These basis sets are internally mapped as fully relativistic (*i.e.*, including the spin-orbit coupling) by solving the Dirac equation of each atom.<sup>42, 43</sup> The SG15-High accuracy basis sets were used with pseudopotential projectorshift (PPS) parameters for Ge. These PPS parameters enable smoothening of the

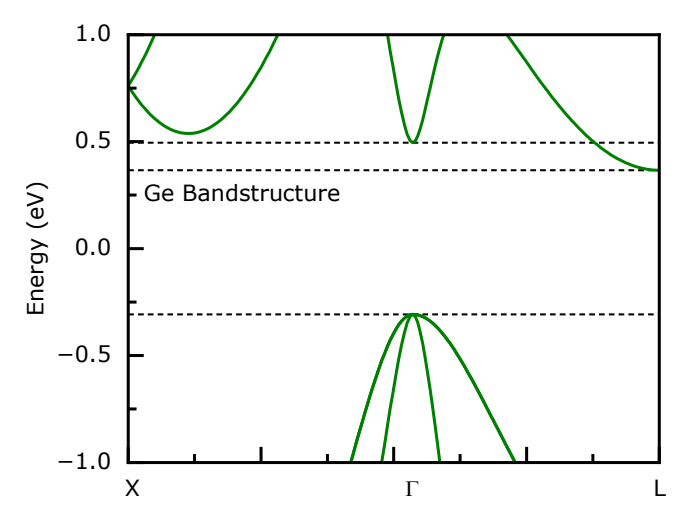


**FIG. 1**. Electronic band structure of bulk Ge computed using the SG15 PPS-PBE pseudopotential method with LCAO (High accuracy) basis set approach, extracting  $E_{g, \Gamma} = 0.802$  eV and  $E_{g, L} = 0.673$  eV from the 2-atom primitive bulk configuration.

oscillations in valence electron wavefunctions in the pseudopotential functional, which improves the accuracy of calculations. However, such additional projector parameters for add-on accuracy in pseudopotentials are available only for Si and Ge atoms in the Synopsys QuantumATK framework. It is noted that SG15-Ultra basis sets are more accurate at the cost of computation speed. The QuantumATK tool includes the PPS-PBE parameters for Si and Ge, correcting the energy band gap obtained from the GGA approximations. This accurately estimates the band gap corresponding to experimental values.<sup>35</sup> Furthermore, calibration of this DFT computation method with the Ge band gap, shown in **Figure 1**, was performed giving direct band gap  $E_{g,T} = 0.802$  eV and indirect band gap  $E_{g,L} = 0.673$  eV. Later, this calibrated DFT method was utilized to compute the electronic band structures of different compositional  $Ge_{1-x}Sn_x$  alloys with and without clusters of Sn atoms.

## B. Computational Details

To investigate Sn clustering in a  $Ge_{1-x}Sn_x$  alloy, a 54-atom bulk supercell configuration was created through a  $3\times3\times3$  repetition of a 2-atom bulk configuration. A

Monkhorst–Pack k-point grid of 3×3×3 and the density Hartree mesh cutoff energy of 100 eV were used, where the SG15 pseudopotential with high accuracy basis sets extracts band gaps that converge to within 10<sup>-4</sup> eV. As for the LCAO high accuracy basis sets, for each orbital of Ge and Sn atom, the radial step size was 0.001 Bohr (i.e. 0.000529 Å) and such high accuracy basis set led total energy convergence to the maximum deviation of 1 meV/atom from Ultra accurate basis set (which itself is 0.1% accurate to the original LCAO basis sets). Moreover, the maximum allowed interaction distance between two orbitals was kept at 20 Å. With maximum 100 self-consistent field (SCF) iterations, the band energies converged to a constant value within  $10^{-4}$  eV between the consecutive steps, where the self-consistent electron density was found. Cluster-free  $Ge_{1-x}Sn_x$  (x = 3.7% to 27.77%) alloy supercells were built with only (i) Ge-Ge and (ii) Ge-Sn bonds in the 54-atom supercell bulk configuration. To study the impact of Sn clustering in GeSn alloy, the supercell was built with (i) Ge-Ge, (ii) Ge-Sn, and (iii) Sn-Sn bonds with Sn atoms clustered only as 1<sup>st</sup>-NNs, as shown in **Figure 2** for x = 22.22%. The present work focused on investigating the effects of Sn clustering over the effective potential, DOS, total energy

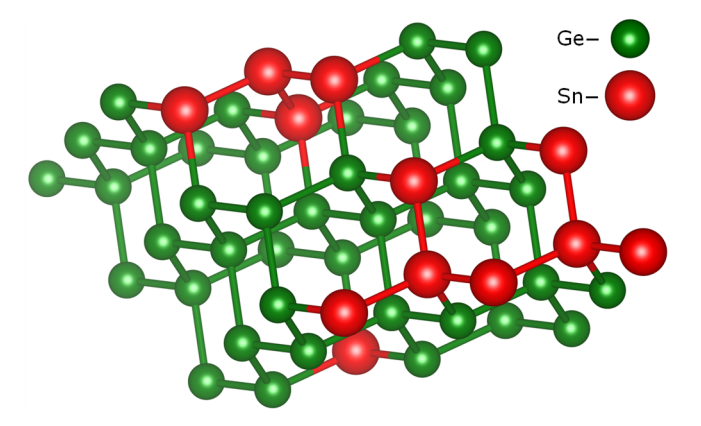


**FIG. 2**. Crystal structure of a 54-atom supercell bulk configuration of Ge<sub>0.7778</sub>Sn<sub>0.2222</sub> built in the Synopsys QuantumATK Builder tool, formed with clustered Sn atoms. Schematic drawn using Vesta.<sup>45</sup>

(deducing the formation energy), and electronic band structure of GeSn. Studies related to the short-range order (SRO) effect observed in GeSn, $^{25,44}$  are outside the scope of this work as neither the random alloy distribution nor the SRO in GeSn depicts the effect of Sn segregation or Sn–Sn clustering as reported. $^{25}$  Moreover, to compute the effective band structure (EBS) of  $Ge_{1-x}Sn_x$  alloy (x = 3.71% to 27.77%) as a primitive cell configuration, the band structure of each 54-atom supercell was unfolded using the spectral weights of the eigen wavefunctions. The fundamental band gaps,  $E_g$ ,  $\Gamma$  and  $E_g$ , L, were determined from the folded electronic band structure of the supercell, and further confirmed from the respective effective band structures of the  $Ge_{1-x}Sn_x$  alloy. Further, the width of the forbidden gap (noticeably the indirect gap till transition and the direct gap at higher Sn composition) was also presented from a separately computed DOS for all bands on either side of the valence band maxima and conduction band minima with Monkhorst–Pack  $3\times3\times3$  **k**-point grid.

#### **III. RESULTS AND DISCUSSION**

#### A. Effective Potential

Effective Potential,  $V_{eff}$ , is the overall potential experienced by the electrons in many electron-system, and the contributing factors of Hartree potential  $V_{H}$ , exchange-correlation potential  $V_{XC}$ , and external potential  $V_{ext}$  were as noted in Eq. (2). As denoted in Eq. (1), the KS Hamiltonian considers  $V_{eff}$  to compute the total energy of the system.  $V_{eff}$  was computed for eleven cluster-free Ge<sub>1-x</sub>Sn<sub>x</sub> (x = 3.71% to 27.77%) and eight 1<sup>st</sup>-NN clustered Ge<sub>1-x</sub>Sn<sub>x</sub> (x = 3.71% to 22.22%) alloy compositions, as a part of the DFT calculations. Shown in **Figure 3** are three representative compositions of 5.56%, 14.81%, and 22.22%, it was noted that  $V_{eff}$  drops in the coordinate positions of Sn atoms clustering

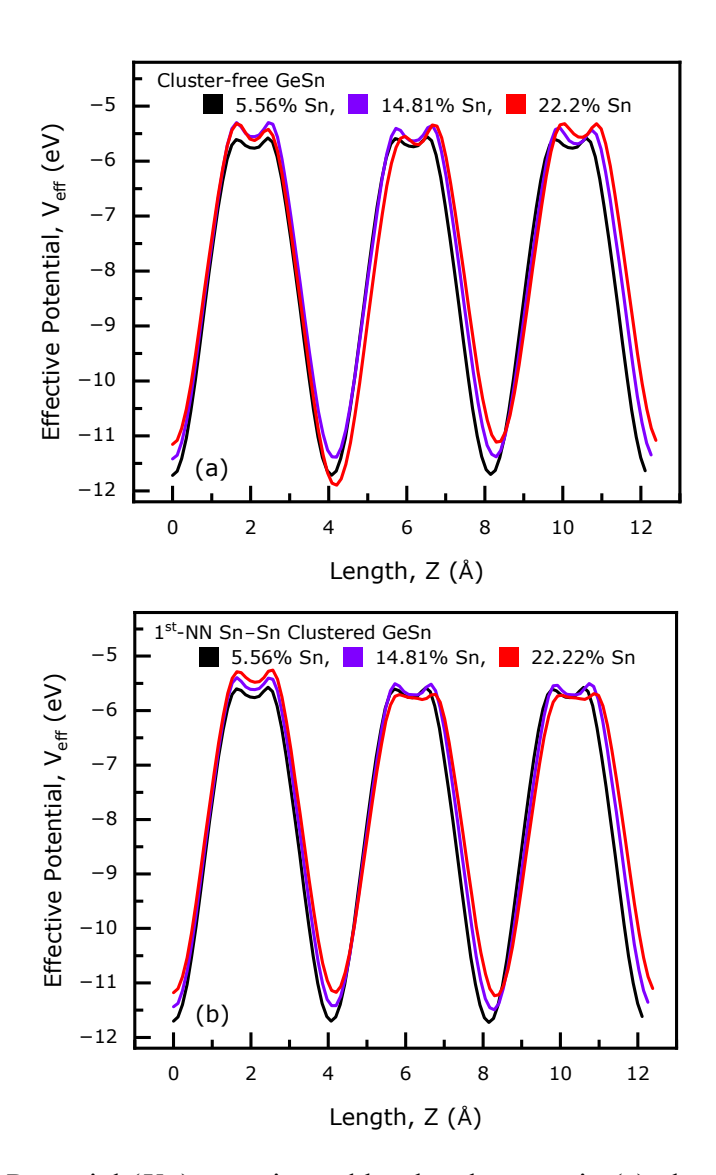


**FIG. 3**. Effective Potential ( $V_{eff}$ ) experienced by the electrons in (a) cluster-free GeSn and (b) 1<sup>st</sup>-NN Sn-Sn clustered GeSn at Sn compositions of 5.56%, 14.81% and 22.22%, represented along the Z-direction. For 22.22% Sn composition, the clustering of Sn atoms decreases the effective potential (see from 8 to 12 Å in (a) and (b)).

together and has decreased periodicity, vividly observed for high Sn composition of 22.22 % where more Sn–Sn bonds were present. This observation was noted in all the directions at coordinates of clustered Sn atoms, though  $V_{eff}$  is shown only for Z-direction here. Such variation in the periodicity of  $V_{eff}$  leads to the decrease in the direct and indirect energy band gaps of GeSn (discussed in *section C*), however, lack of controllability over Sn–Sn

clustering makes it an unintended property of the GeSn material system. Moreover, it leads to variation in the localized Sn composition and the average Sn composition of the material, based on the density of clusters. <sup>26–28</sup> Such Sn clustering is widely reported during the synthesis of GeSn material systems, <sup>19–22, 25, 44</sup> where clustering of Sn atoms makes the targeted band gaps deviate from the design parameters. In turn, 1<sup>st</sup>-NN clustering of Sn atoms was selectively investigated for each composition of GeSn alloy in the present work, due to the distributive nature of Sn clustering in epitaxial GeSn from 1<sup>st</sup>-NN to 4<sup>th</sup>-NN Sn clusters observed from APT measurements showing 1<sup>st</sup>-NN Sn–Sn as peak cluster. <sup>26</sup> This leads to different regions of a thin film GeSn to exhibit different electronic and optical properties. <sup>19–22, 25, 44</sup>

## B. Thermodynamic stability

The stability of the GeSn material system during the fabrication remains one of the primary concerns due to Sn segregation or clustering in various process steps.  $^{19-22}$  Here, the thermodynamic stability of the GeSn alloy was studied by computationally arriving at the formation energy comparison between the cluster-free and  $1^{st}$ -NN Sn–Sn clustered GeSn alloy, as mathematically represented in Section II-A. As shown in Table I,  $E_{Total}$  of the clustered Ge<sub>1-x</sub>Sn<sub>x</sub> alloy is higher, and so is the  $E_{Form}$ , thereby decreasing the thermodynamic stability of the system. It is imperative to note that, in a 5-atom GeSn cluster, SnGe<sub>4</sub> is identified as the most stable cluster.  $^{24}$  Moreover, the binding energy of the bonds Ge–Ge > Ge–Sn > Sn–Sn supports better thermodynamic stability  $^{24}$  (higher binding energy correlates to better stability) as also shown by the computation results in the present work. These characteristics were more clearly observed at higher Sn compositions, where the difference in the individual contributing energy terms of  $E_H$  and

**TABLE I.** Total Energy difference ( $\Delta E_{Total}$ ), equivalent to formation energy difference ( $\Delta E_{Form}$ ), of 1<sup>st</sup>-NN Sn–Sn clustered and cluster-free 54-atom Ge<sub>1-x</sub>Sn<sub>x</sub> supercell bulk configuration for compositions from 3.7% to 22.22%, with individual energy differences of Kinetic ( $\Delta T$ ), Electrostatic ( $\Delta E_H$ ), and Exchange-correlation ( $\Delta E_{XC}$ ) energies. [All differences are (Clustered) – (Cluster-free)]

Sn comp. (%)	$\Delta T (\text{eV})$	$\Delta E_H (eV)$	$\Delta Exc$ (eV)	$\Delta E_{Total} = \Delta E_{Form} (eV)$
3.7	- 0.54	0.77	0.037	0.270
5.56	- 1.03	1.50	0.059	0.535
7.41	- 1.48	2.18	0.086	0.789
11.11	- 2.55	3.73	0.120	1.294
12.96	- 3.05	4.46	0.142	1.544
14.81	- 3.57	5.22	0.140	1.785
18.52	- 4.56	6.61	0.194	2.239
22.22	- 5.58	8.03	0.224	2.671

 $E_{XC}$  continues to increase with increased Sn clustering. Contribution from the potential energy of an electron due to the interaction with other electrons, *i.e.* the  $E_H$  is more pronounced. The effect of local electron density n(r) and local gradient of electron density,  $\nabla n(r)$ , due to 1<sup>st</sup>-NN clustered Sn–Sn atoms increases the  $E_{XC}$  energy as denoted by Eq. (7), even if less than  $E_H$  as noted from Eq. (6). Certainly, such an increased  $E_{Total}$  (increased  $E_{Form}$ ) affects the ground state of the system that is used to compute the electron density (n), iteratively, electronic band structure, and the direct-indirect energy band gaps of the  $Ge_{1-x}Sn_x$  alloy. With the 54-atom supercell configuration, the unfolded effective band

structure as well as the density of states of the 1<sup>st</sup>-NN Sn-Sn clustered Ge<sub>1-x</sub>Sn<sub>x</sub> alloy presented in the next section highlights these effects.

## C. Band Structure and Density of States

The electronic band structure of supercells contains hundreds of electronic bands that need unfolding to determine the effective band structure of the primitive cell configuration for the Ge<sub>1-x</sub>Sn<sub>x</sub> alloy at each composition.<sup>46</sup> Here, with 1<sup>st</sup>-NN Sn–Sn clusters in 54-atom GeSn supercell, it becomes even more essential to observe the effective band structure. Wherein, the eigen functions of the wavefunctions in the LCAO basis set

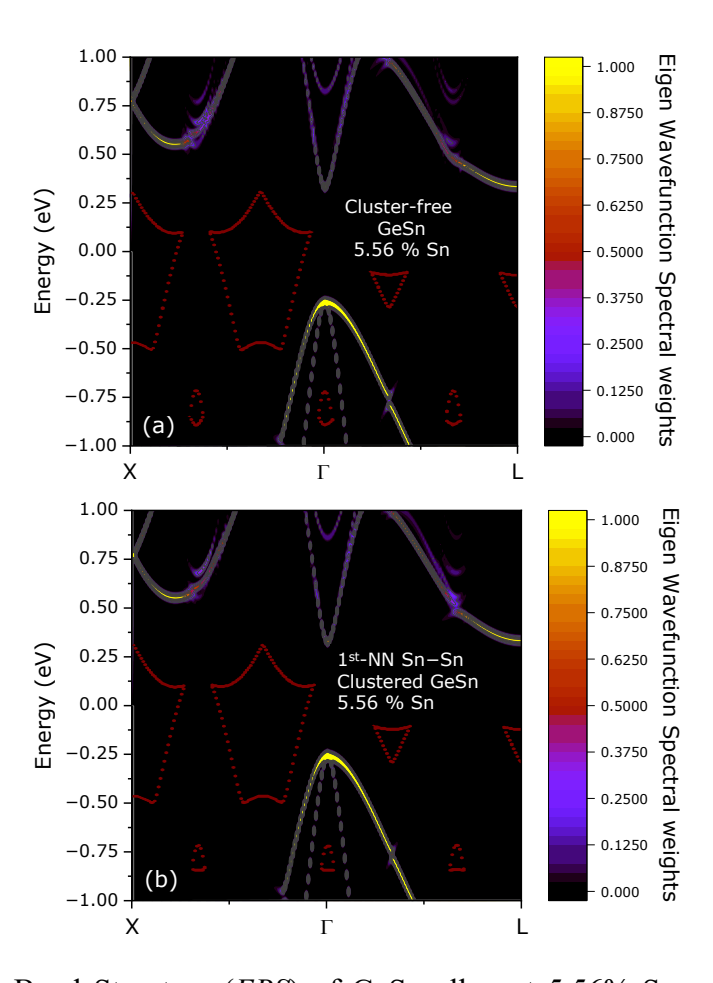


**FIG. 4**. Effective Band Structure (*EBS*) of GeSn alloy at 5.56% Sn composition as (a) Cluster-free and (b) 1<sup>st</sup>-NN Sn–Sn clustered GeSn.  $E_{g, \Gamma}$  drops by 0.5 meV and  $E_{g, L}$  by 12.8 meV due to Sn clustering at 5.56%.

approach are assigned weights at each **k**-point of the supercell, where DFT computation is executed. **Figure 4** shows the *EBS* of cluster-free and clustered GeSn for 5.56% Sn. At low Sn composition, the reduction in the band gaps  $[\Delta E_g, \Gamma = 0.5 \text{ meV}, \Delta E_g, L = 12.8 \text{ meV}]$  is less than at the high Sn compositions such as 22.22%  $[\Delta E_g, \Gamma = 40.76 \text{ meV}, \Delta E_g, L = 120.17 \text{ meV}]$  shown in **Figure 5**, that has  $E_g, \Gamma$  cluster-free = 0.17 eV. With clustering at higher Sn composition,  $n(\mathbf{r})$  adds more weightage to the drop in the band gaps than at lower Sn composition. This characteristic is observed for clustering from 3.7 % to 22.22% and even

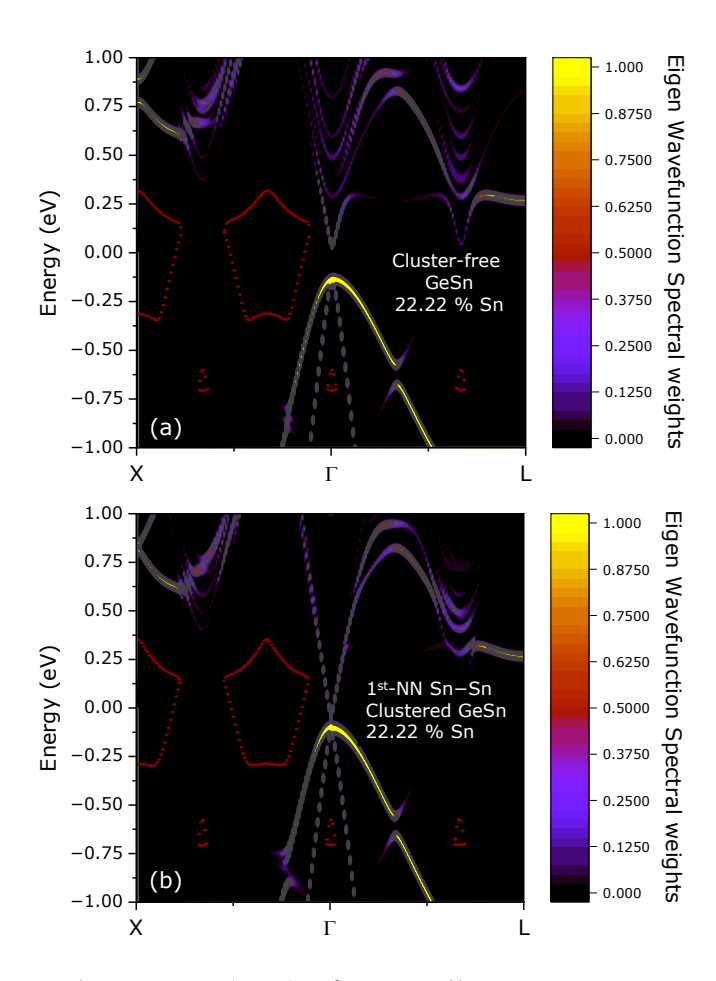


**FIG. 5**. Effective Band Structure (*EBS*) of GeSn alloy at 22.22% Sn composition as (a) Cluster-free and (b) 1<sup>st</sup>-NN Sn–Sn clustered GeSn. Direct band gap,  $E_g$ ,  $\Gamma$ , drops by 40.76 meV and indirect band gap,  $E_g$ , L, by 120.17 meV due to Sn clustering at 22.22%, where  $E_g$ ,  $\Gamma$  clustered = 0.05 eV.

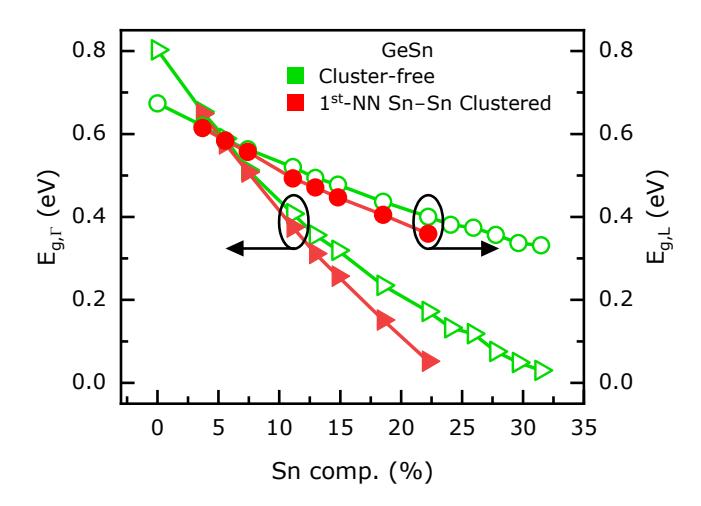


**FIG. 6**. Decrease in the direct band gap,  $E_{g, \Gamma}$  ( $\Delta$ -symbol), and indirect band gap,  $E_{g, L}$  ( $\circ$ -symbol) energies due to Sn clustering increases with increasing Sn composition, as observed for cluster-free (*green color*) and 1<sup>st</sup>-NN Sn-Sn clustered (*red color*) GeSn.

beyond, though the energy band gaps shown in **Figure 6** were not computed for clustering beyond 22.22% as  $E_g$ ,  $\Gamma$  clustered becomes 0.05 eV there itself. Moreover at 27.77% Sn, the  $E_g$ ,  $\Gamma$  cluster-free = 0.075 eV. Note that by no means, it is claimed in the present work that Ge<sub>1-x</sub>Sn<sub>x</sub> reaches 0 eV band gap at 27.77%, as with the ordering effects reported in literature<sup>18</sup>, <sup>25,44</sup> even at 32% Sn band gaps 0.15 eV have been calculated, and at 28% band gap crossing 0 eV has also been reported.<sup>2,16,17</sup> These deviations due to ordering effects still exist within the Ge<sub>1-x</sub>Sn<sub>x</sub> alloy system that is not observed in Si<sub>1-x</sub>Ge<sub>x</sub> material systems or the III-V semiconductors that behave as a truly random alloy.<sup>25</sup>

This characteristic nature of Sn clustering in the  $Ge_{1-x}Sn_x$  alloy was observed from DOS as well, in a separate computation from band structure calculations, at each **k**-point using Monkhorst–Pack **k**-point grid of  $3\times3\times3$ . Presenting for x=5.56% and 22.22% in **Figure 7** as representatives of similar observations noted in other compositions. Evident from **Figure 7** (b) is the rise in DOS and hence the reduction in the width of the forbidden gap due to the  $1^{st}$ -NN Sn–Sn clustering in 22.22 % (high composition). Similar

characteristics were reported from the band gaps and effective band structures as noted in **Figures 4–6**, further proving the variation in the energy band gaps at a fixed Sn composition based on the well-dispersed Sn atoms or clustered Sn atoms.

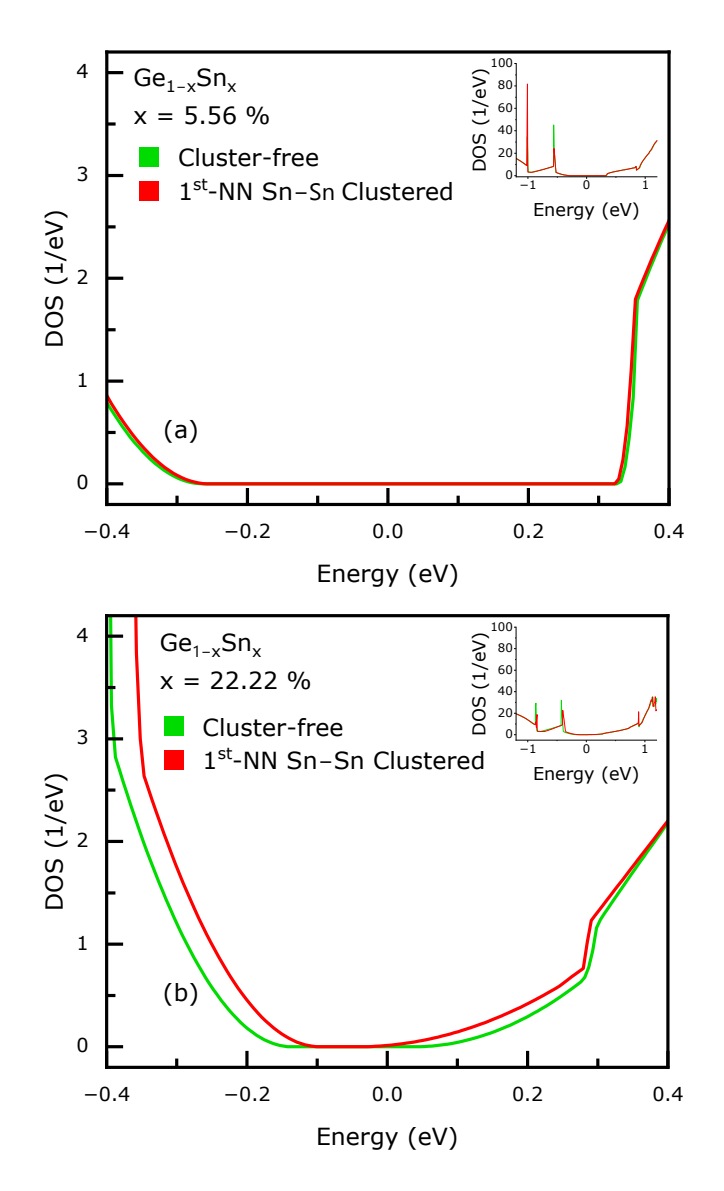


FIG. 7. Density of States (*DOS*) of  $Ge_{1-x}Sn_x$  alloy at (a) x = 5.56 % and (b) x = 22.22 %. The width of the forbidden gap decreases with 1<sup>st</sup>-NN Sn–Sn clustering in  $Ge_{1-x}Sn_x$ , indicating decrease in the band gap. At x = 22.22%, GeSn is fully direct with the observed *DOS* belonging to direct band  $\Gamma$ , whereas at x = 5.56%, GeSn is yet to become direct, yet so close that the *DOS* is apparently from both direct and indirect bands.

#### IV. SUMMARY AND CONCLUSIONS

In conclusion, we have shown that the 1<sup>st</sup>-NN Sn–Sn clustering in GeSn alloy has a significant effect on the electronic band structure and thermodynamic stability, thereby modifying the fundamental material properties of direct and indirect energy band gap in a GeSn alloy. The clustering effect increased the formation energy and reduced the thermodynamic stability of GeSn by increasing both Hartree potential energy and exchange-correlation potential energy. In addition, it reduced both indirect and direct band gap energies, more significantly at higher Sn compositions. For instance, with 1st-NN Sn-Sn clustered GeSn at a Sn composition of ~22%,  $E_{g, \Gamma}$  and  $E_{g, L}$  band gaps decreased by 40.76 meV and 120.17 meV, respectively. In addition, from the separately computed density of states, it was observed that the width of the forbidden band gap reduced with Sn clustering. This supports the requirement to characterize and identify the clustering in GeSn material systems prior to reporting the accurate direct-indirect energy band gaps at a particular composition and prevent process variation effects in the device and circuit performance parameters. Hence, it is prudent to initiate revisions in the first-principles calculations for the direct and indirect energy band gaps of GeSn alloy with the effect the of Sn-Sn clustering incorporated.

## **ACKNOWLEDGMENTS**

The authors thank John K. Ghra (Systems Administrator for ECE, Virginia Tech) for assistance in computational services.

#### **AUTHOR DECLARATIONS**

#### **Conflicts of Interest (required)**

The authors have no conflicts to disclose.

#### DATA AVAILABILITY

The data that support the findings of this study are available from the corresponding author upon reasonable request.

## **REFERENCES**

- <sup>1</sup>K. Wada and L. C. Kimerling, *Photonics and Electronics with Germanium* (Wiley-VCH, Weinheim, 2015).
- <sup>2</sup>S. Gupta, B. Magyari-Köpe, Y. Nishi, and K. C. Saraswat, J. Appl. Phys. **113**, 073707 (2013).
- <sup>3</sup>O. Moutanabbir et al., Appl. Phys. Lett. **118**, 110502 (2021).
- <sup>4</sup>C. Sun *et al.*, Nature **528**, 534 (2015).
- <sup>5</sup>A. Elbaz et al., Nat. Photonics **14**, 375 (2020).
- <sup>6</sup>S. Wirths *et al.*, Nat. Photonics **9**, 88 (2015).
- <sup>7</sup>C.-Y. Chang, R. Bansal, K.-C. Lee, G. Sun, R. Soref, H. H. Cheng, and G.-E. Chang, Opt. Lett. **46**, 3316 (2021).
- <sup>8</sup>R. Chen, S. Gupta, Y.-C. Huang, Y. Huo, C. W. Rudy, E. Sanchez, Y. Kim, T. I. Kamins, K. C. Saraswat, and J. S. Harris, Nano. Lett. **14**, 37 (2014).

- <sup>9</sup>S. Xu, W. Wang, Y.-C. Huang, Y. Dong, S. Masudy-Panah, H. Wang, X. Gong, and Y.-C. Yeo, Opt. Express 27, 5798 (2019).
- <sup>10</sup>K.-C. Lee, M.-X. Lin, H. Li, H.-H. Cheng, G. Sun, R. Soref, J. R. Hendrickson, K.-M. Hung, P. Scajev, and A. Medvids, Appl. Phys. Lett. 117, 012102 (2020).
- <sup>11</sup>H. Tran et al., ACS Photonics **6**, 2807 (2019).
- <sup>12</sup>J. Liu, X. Sun, D. Pan, X. Wang, L. C. Kimerling, T. L. Koch, and J. Michel, Opt. Express 15, 11272, (2007).
- <sup>13</sup>M. K. Hudait, F. Murphy-Armando, D. Saladukha, M. B. Clavel, P. S. Goley, D. Maurya, S. Bhattacharya, and T. J. Ochalski, ACS Appl. Electr. Mater. 3, 4535 (2021).
- <sup>14</sup>M. B. Clavel, F. Murphy-Armando, Y. Xie, K.T. Henry, M. Kuhn, R. J. Bodnar, G. A. Khodaparast, D. Smirnov, J. J. Heremans, and M.K. Hudait, Phys. Rev. Appl. 18, 064083 (2022).
- <sup>15</sup>R. Joshi, S. Johnston, S. Karthikeyan, L. F. Lester and M. K. Hudait, IEEE J. Sel. Top. Quant. **30**,1 (2024).
- <sup>16</sup>C. Eckhardt, K. Hummer, and G. Kresse, Phys. Rev. B. **89**, 165201 (2014).
- <sup>17</sup>M. P. Polak, P. Scharoch and R. Kudrawiec, J. Phys. D Appl. Phys. **50**,195103 (2017).
- <sup>18</sup>C. Xu, D. Ringwala, D. Wang, L. Liu, C. D. Poweleit, S. L. Y. Chang, H. L. Zhuang, J. Menéndez, and J. Kouvetakis, Chem. Mater. 31, 9831 (2019).
- <sup>19</sup>T. Liu, L. Wang, G. Zhu, X. Hu, Z. Dong, Z. Zhong, Q. Jia, X. Yang and Z. Jiang, Semicond.
  Sci. Tech. 33, 125022 (2018).
- <sup>20</sup>P. Ščajev, V. Soriūtė, G. Kreiza, T. Malinauskas, S. Stanionytė, P. Onufrijevs, A. Medvids, and H.-H. Cheng, J. Appl. Phys. 128, 115103 (2020).

- <sup>21</sup>M. K. Hudait, S. W. Johnston, M. B. Clavel, S. Bhattacharya, S. Karthikeyan, and R. Joshi, J. Mater. Chem. C 10, 10530 (2022).
- <sup>22</sup>E. Rogowicz, J. Kopaczek, J. Kutrowska-Girzycka, M. Myronov, R. Kudrawiec, and M. Syperek, ACS Appl. Electr. Mater. **3**, 344 (2021).
- <sup>23</sup>J.-G. Han, P.-F. Zhang, Q.-X. Li, H. Gao, G.-Y. Cao, L.-S. Sheng, and Y.-W. Zhang, J. Mol. Struc-Theochem 624, 257 (2003).
- <sup>24</sup>P. N. Samanta and K. K. Das, Comput. Theor. Chem. **980**, 123 (2012).
- <sup>25</sup>B. Cao, S. Chen, X. Jin, J. Liu, and T. Li, ACS Appl. Mater. Inter. 12, 57245 (2020).
- <sup>26</sup>A. Kumar, M. P. Komalan, H. Lenka, A. K. Kambhama, M. Gilberta, F. Gencarelli, B. Vincent, and W. Vandervorst, *Ultramicroscopy* **132**, 171 (2013).
- <sup>27</sup>A. Kumar, J. Demeulemeester, J. Bogdanowicz, J. Bran, D. Melkonyan, C. Fleischmann, F. Gencarelli, Y. Shimura, W. Wang, R. Loo, and W. Vandervorst, J. Appl. Phys. 118, 025302 (2015).
- <sup>28</sup>F. Gencarelli, D. Grandjean, Y. Shimura, B. Vincent, D. Banerjee, A. Vantomme, W. Vandervorst, R. Loo, M. Heyns, and K. Temst, J. Appl. Phys. 117, 095702 (2015).
- <sup>29</sup>S. Smidstrup *et al.*, J. Phys-Condens. Mat. **32**, 015901 (2020).
- <sup>30</sup>K. Wang, X. Zhang, and F. Wang, Chem. Phys. Lett. **836**, 141024 (2024).
- <sup>31</sup>B. Liu, R. Tian, H. Yu, L. He, L. Yang, F. Wang, H. Geng, and Y. Tian, Eng. Fail. Anal. 159 108145 (2024).
- <sup>32</sup>P. Hohenberg and W. Kohn, *Phy. Rev.* **136**, B864 (1964).
- <sup>33</sup>W. Kohn and L. J. Sham, *Phys. Rev.* **140**, A1133 (1965).
- <sup>34</sup>W. Kohn, A. D. Becke and R. G. Parr, J. Phys. Chem.-US **100**, 12974 (1996).

- <sup>35</sup>S. Smidstrup, D. Stradi, J. Wellendorff, P. A. Khomyakov, U. G. Vej-Hansen, M. -E. Lee, T. Ghosh, E. Jónsson, H. Jónsson, and K. Stokbro, Phys. Rev. B. 96, 195309 (2017).
- <sup>36</sup>See https://www.synopsys.com/silicon/quantumatk.html for QuantumATK version U-2022.12-SP1, Synopsys QuantumATK.
- <sup>37</sup>C. Li, X. Zhang, and F. Wang, Vacuum **220**, 112793 (2024).
- <sup>38</sup>C. J. Bartel, A. Trewartha, Q. Wang, A. Dunn, A. Jain, and G. Ceder, npj Comput. Mater. 6, 97 (2020).
- <sup>39</sup>S. Kirklin, J. E. Saal, B. Meredig, A. Thompson, J. W. Doak, M. Aykol, S. Rühl and C. Wolverton, npj Comput. Mater. 1, 15010 (2015).
- <sup>40</sup>F. El-Mellouhi and N. Mousseau, Phys. Rev. B. 71, 125207 (2005).
- <sup>41</sup>S. B. Zhang and J. E. Northrup, Phys. Rev. Lett. **67**, 2339 (1991).
- <sup>42</sup>A. Dal. Corso and A. M. Conte, Phys. Rev. B. **71**, 115106 (2005).
- <sup>43</sup>G. Theurich and N. A. Hill, Phys. Rev. B. **64**, 073106 (2001).
- <sup>44</sup>X. Jin, S. Chen, and T. Li, Commun. Mater. **3**, 66 (2022).
- <sup>45</sup>K. Momma and F. Izumi, J. Appl. Crystallogr. **44**, 1272 (2011).
- <sup>46</sup>V. Popescu and A. Zunger, Phys. Rev. Lett. **104**, 236403 (2010).